

Excitation of interstellar molecules by near infrared PAH photons

M. Giard¹, J.L. Puget², E. Cr  t  ¹, F. Scoupe¹

¹ Centre d'Etude Spatiale des Rayonnements, 9 avenue du Colonel Roche, BP 4346, F-31029 Toulouse Cedex, France.

² Institut d'Astrophysique Spatiale, Campus d'Orsay, B  t. 121, F-91405 Orsay cedex, France.

Received ; accepted

Abstract.

We have developed an excitation model for small molecules including radiative pumping by dust photons from near infrared to submillimeter wavelengths. This model applies to molecules within bright photodissociation regions in galactic star-forming regions and starburst galaxies. In such environments, the near infrared photons emitted by polycyclic aromatic hydrocarbon molecules (PAHs) or small carbon grains, $5 \mu\text{m} < \lambda < 20 \mu\text{m}$, are able to penetrate molecular regions and pump the molecules in an excited vibration state. The far infrared and submillimeter transitions involved in the de-excitation cascade are strongly affected by this process. Their intensities can be enhanced by several orders of magnitude. We have applied this model to H_2O and NH_3 , ortho and para species. The behaviour of the FIR rotation lines with respect to the gas density and the molecule column density is strongly modified compared to pure collisional models. At moderate densities, $n_{H_2} < 10^5 \text{ cm}^{-3}$, radiative pumping dominates the excitation of the rotation ladder, and the FIR lines are good probes of the molecule column density. The near infrared absorption and emission lines predicted to appear between 6 and 7 μm for H_2O and from 10 to 12 μm for NH_3 can also be used for this purpose. Concerning *ortho* - H_2O , a quasi resonant pumping of the ν_2 6.18 μm transition by photons of the 6.2 μm PAH band occurs. A strong de-excitation emission line is expected at 6.64 μm .

Key words: dust - ISM: molecules - ISM:clouds - reflection nebulae - Infrared:ISM:lines and bands - Galaxies:starburst

1. Introduction

Modelling the formation of molecular rotation lines in interstellar clouds is a crucial task both for theoretical and observational astrophysics. On the theoretical side, early studies by Goldreich and Kwan (1974) and Goldsmith and Langer (1978) have shown that the rotation lines from polar and/or abundant molecules like CO , O_2 , HD , H_2O and other hydrides should be the major cooling agents of the molecular gas. Together with the heating mechanisms (e.g. cosmic rays, H_2 for-

mation, gravitational contraction and grain heating), they control the thermal balance of dense clouds, and thus, the conditions that will allow the contraction toward star formation. On the observational side, millimeter and submillimeter molecular lines are used to probe several physical parameters of molecular clouds, such as the gas temperature, the H_2 density, the abundance of molecules, and the gas dynamics. Densities and temperatures in molecular clouds are such that the collision rate with H_2 molecules generally does not allow to reach the thermodynamic equilibrium of the rotation ladder (see Goldreich and Kwan 1974). Instead, the coupling with the radiation field is important, both via absorption and spontaneous emission. Takahashi et al. (1983 and 1985), have shown how far infrared dust photons, $\lambda = 30$ to $100 \mu\text{m}$ are able to pump the rotation ladder of the H_2O molecule within warm molecular cores. Carroll and Goldsmith (1981) have investigated the pumping of molecules via their near infrared (NIR) vibration transitions. At that time it was assumed that a significant fraction of the dust emission could be in the NIR range, only in the immediate vicinity of hot stars. However, the effect of the NIR radiation attributed to large polycyclic aromatic hydrocarbon molecules (PAHs) and very small grains, which makes up to 30 % of the total dust emission (Puget et al. 1985), has never been taken into account. This radiation is characterised by a strong continuum and broad emission features, located at 6.2 and 7.7 μm for the strongest ones, wavelengths which coincide with the vibration transitions of some molecules. For instance the ν_2 transition of H_2O and the ν_4 transition of NH_3 occur at the maximum of the 6.2 μm PAH feature, and the 7.8 μm vibration of CS falls within the wavelength range of the 7.7 μm feature. There is now clear observational evidence that the NIR emission bands are not only present in peculiar reflexion nebulae, but are a general component of the dust radiation: detection of the 3.3 and 6.2 μm bands in our galaxy by Giard et al. 1994a and Ristorcelli et al. 1994, and, more recently, the measurements performed by the ISO satellite (Boulanger et al. 1996, Mattila et al. 1996, and Verstraete et al. 1996). The aim of this paper is to revisit the problem of the coupling between molecules and the dust radiation field, in the framework of a model which includes the PAH emission bands. The mechanism, and the rates involved in some representative astrophysical environments, are presented in Sect. 2. A detailed model for the molecular excitation in star-forming photodissociation regions (PDR) is developed in Sect. 3. The results for

Send offprint requests to: M. Giard, giard@cesr.cnes.fr

two molecules, H_2O and NH_3 , are presented in Sect. 4.

2. Near infrared pumping of rotation transitions

Near infrared (NIR) PAH photons, continuum or bands, can excite the vibrations of a molecule. This absorption does also imply some rotational excitation ($\Delta J \neq 0$). After spontaneous de-excitation of the vibration mode, which occurs almost immediately ($A_{ij} \simeq 10 \text{ s}^{-1}$), the molecule can be left in an excited rotation state. Subsequent excitation from this state to an upper one can follow via the same mechanism. We have listed in Table 1 some molecules of astrophysical interest which may be affected by this process, because one of the vibration transitions happen to be at a wavelength larger than $6 \mu\text{m}$ ($< 1670 \text{ cm}^{-1}$), where the PAH emission is strong.

Table 1. Some molecules of astrophysical interest which happen to have one or several vibration transitions that can be pumped by PAH photons. Frequencies and Einstein coefficients are from the compilation of Encrenaz et al. 1992. If not available the Einstein coefficient has been approximated to 10 s^{-1} . Column 4: indicative abundance relative to hydrogen. When available, we have used the value from the dust/gas chemical model of Shalabiea and Greenberg 1994 at a time evolution of 10^6 years. The abundance of H_3O^+ is from Phillips et al. 1993. Column 5: optical depth in the absorbing vibration transition for a typical PDR column density: $2 N_{H_2} = 10^{21} \text{ cm}^{-2} (\text{km/s})^{-1}$.

Molecule	ν_{vib} cm^{-1}	A_{vib} s^{-1}	Abundance	τ
H_2O	ν_2 1620	20	10^{-5}	19
NH_3	ν_2 950	16	10^{-6}	7
	ν_4 1627	5		0.5
CO_2	ν_2 670	1.4	10^{-6}	2
C_3H_2 (cyclic)	ν_3 1277	10	$2 \cdot 10^{-8}$	0.04
CH_4	ν_4 1306	2.6	10^{-6}	0.5
HCN	ν_2 712	1.7	10^{-6}	2
HC_3N	ν_5 663	4.7	10^{-9}	0.006
H_3O^+	ν_4 1626	10	$3 \cdot 10^{-9}$	0.003
CH_3OH	$\nu_4 \dots \nu_8, \nu_{10}, \nu_{11}$	10	$3 \cdot 10^{-7}$	1.2
	1033 ... 1478			
CS	1285	10	$3 \cdot 10^{-6}$	5.5

In order to get a first quantitative estimate of the competition between the proposed mechanism (radiative NIR pumping) and collisional excitation, we have to figure out what are the rates of each elementary process. Concerning the effect of collisions with H_2 , the deexcitation rate is approximately (see Goldreich and Kwan 1974) :

$$\frac{k_{col.deexc.}^{-1}}{\text{s}^{-1}} \simeq 7 \cdot 10^{-7} \left(\frac{T}{100K} \right)^{0.5} \frac{n_{H_2}}{10^4 \text{ cm}^{-3}} \quad (1)$$

where T is the gas temperature, and n_{H_2} the gas density. The excitation rate follows from the detailed balance:

$$\frac{k_{col.exc.}^{-1}}{\text{s}^{-1}} \simeq k_{col.deexc.}^{-1} \frac{g_u}{g_l} \exp(-(E_u - E_l)/kT) \quad (2)$$

where g_u , E_u (respectively g_l , E_l) are the statistical weight and the energy of the upper (respectively lower) level.

The radiative excitation rate is given by the product of the Einstein coefficient by the spectral radiation density:

$$\frac{k_{rad}^{-1}}{\text{s}^{-1}} \simeq 6.8 \cdot 10^{-7} \frac{A_{ul}}{\text{s}^{-1}} \frac{\langle I_\nu \rangle}{\text{MJy/sr}} \left(\frac{\nu}{10^{12} \text{ Hz}} \right)^{-3} \quad (3)$$

where A_{ul} is the spontaneous emission rate, $\langle I_\nu \rangle$ is the average spectral density of the radiation field in the line (average over frequency and solid angle). The spectral density at the maximum of the 6.2 and 7.7 μm PAH features is a few 10^4 MJy/sr within typical photodissociation regions (PDRs) associated to star forming complexes (e.g. M17, see Girard et al. 1992, and 1994b,) or starburst galaxies. This implies that in such regions and their vicinity, the radiative excitation rate to the vibration excited state, $\simeq 3 \cdot 10^{-6} \text{ s}^{-1}$, can be higher than the collision excitation rate of the rotation ladder, $\simeq 7 \cdot 10^{-7} \text{ s}^{-1}$. Table 2 compares the radiative and collisional rates obtained in the case of the excitation of the 2_{21} rotation level of *ortho* - H_2O , 111 cm^{-1} above the ground state. Fig. 3a shows in detail how this level can be excited via radiative excitation at 6.18 μm of the ν_2 1_{10} state, and spontaneous emission, $A_{ij} \simeq 10 \text{ s}^{-1}$. We have considered different astrophysical environments where radiation can play a significant role: a typical HII/ H_2 galactic PDR in a region of massive star formation (see Tielens and Hollenbach 1985); a molecular cloud nearby to this PDR (e.g. M17 SW); the central regions of a starburst galaxy (e.g. M82); and cold molecular gas within the galactic molecular ring. In the last case, the low value of the radiation field is balanced by the poor collisional efficiency at low temperatures, $T = 50 \text{ K}$. The collision rates are from Green et al. 1993. The figures in this table are only given to illustrate the fact that in such astrophysical environments radiative excitation by NIR PAH photons efficiently competes with collisional excitation. A correct treatment has to take into account the escape probability of the photons from the cloud. This will be done in the next section.

Table 2. Excitation of the 2_{21} rotation level of *ortho* - H_2O , 111 cm^{-1} above the ground level, for different astrophysical environments. k_{col}^{-1} , direct collisional rate from the ground level (Green et al. 1993). k_{rad}^{-1} , radiative excitation rate via the ν_2 1_{10} vibration state (absorption of a 6.18 μm photon).

	$\langle I_\nu \rangle$ MJy/sr	T K	n_{H_2} cm^{-3}	k_{col}^{-1} s^{-1}	k_{rad}^{-1} s^{-1}
PDR	$3 \cdot 10^4$	120	10^4	$6.4 \cdot 10^{-9}$	$1.8 \cdot 10^{-6}$
M17 SW	$1.5 \cdot 10^4$	50	10^5	$3.7 \cdot 10^{-9}$	$0.9 \cdot 10^{-6}$
Starburst	10^4	120	10^4	$6.4 \cdot 10^{-9}$	$6.0 \cdot 10^{-7}$
Gal. H_2	40	50	10^4	$3.7 \cdot 10^{-10}$	$2.4 \cdot 10^{-9}$

3. The model

Our model solves the equations of statistical equilibrium for a given molecule, including rotation levels in the ground and first excited vibration states, assuming an homogenous gas cloud (ie the excitation of the molecule doesn't vary across the cloud) :

$$\begin{aligned} \frac{dx_i}{dt} &= -x_i \sum_{j \neq i} (C_{ij} n_{H_2} + R_{ij}) + \sum_{j \neq i} x_j (C_{ji} n_{H_2} + R_{ji}) \\ &= 0 \end{aligned} \quad (4)$$

where x_i is the molecular fraction in each energy level ($\sum_i x_i = 1$), C_{ij} ($cm^{-3}s^{-1}$) are the collision rates, R_{ij} (s^{-1}) the radiative rates and ν_{ij} the photon frequency of the transition. The radiative transition rates read:

$$\begin{aligned} R_{ij} &= A_{ij} \left(1 + \frac{c^2}{2h\nu_{ij}^3} \langle I_\nu \rangle\right) \quad \text{for } i > j \\ R_{ij} &= A_{ji} \frac{c^2}{2h\nu_{ji}^3} \frac{g_j}{g_i} \langle I_\nu \rangle \quad \text{for } i < j \end{aligned} \quad (5)$$

$\langle I_\nu \rangle$ is the averaged spectral density of the radiation field at the frequency of the transition. This average has to be performed both over the velocity distribution of the molecules, and over the solid angles.

Concerning the radiative transfer, we assume that the PDR is a clumpy medium at small scale, with molecular clumps embedded in a lower density interclump gas, $n_H = 10^3$ to $10^4 cm^{-3}$. There are several observational evidences which support this hypothesis, among which one can cite: 1/ the high CI and CII column densities measured toward the M17-SW PDR and molecular cloud by Genzel et al. 1988 and Stutzki et al. 1988, and 2/ the extension of the PAH emission in the Orion bar, which shows that the UV flux penetrates much deeper into the molecular cloud than what is allowed by extinction in a homogeneous gas (see Tielens et al. 1993 and Giard et al. 1994b). We assume in the following that the UV radiation is converted to near infrared PAH photons in the interclump medium and the outer parts of the molecular clumps, the molecules being at larger A_v behind the dissociation limit. The peculiarity of our problem, compared to the usual line transfer within a dust cloud (see Takahashi et al. 1983 and Collison and Watson 1995), is that the dust component responsible for the near infrared exciting radiation (the PAHs) is not at thermal equilibrium. Here we didn't try to take into account the absorption and emission by dust in a selfconsistent way. Instead, we have neglected the absorption by dust and we use for the dust radiation field the model of Désert et al. 1990, with the flux scaled on the $3.3 \mu m$ measurements of Giard et al. 1994b on M17 South-West and the Orion bar. The only extinction is then the one of the molecules into the clumps. We can use for the dust photons a radiative transfer of the form $(1 - \exp(-\tau))/\tau$, which has been shown to be a good approximation for a medium with absorbing clumps and transparent intercloud phase (see Appendix A in Giard et al. 1992). However, the uncertainty introduced in the model by the transfer used for the dust photons is attenuated by the integration over the line profile which follows in Equ. 10 below.

With such hypothesis the transfer equation reads:

$$I_\nu = S(1 - \exp(-\tau)) + F_d \frac{(1 - \exp(-\tau))}{\tau} \quad (6)$$

where F_d is the dust and PAHs spectral density in the continuum, and S is the line source function:

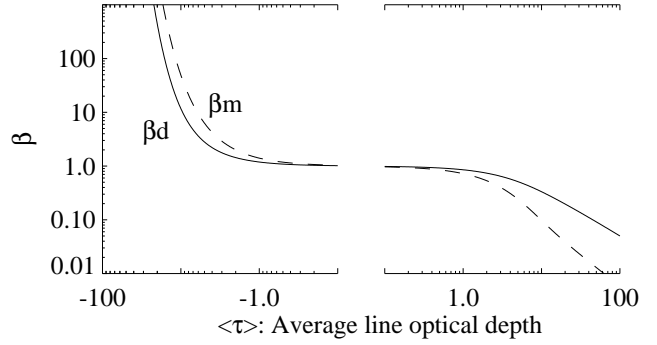


Fig. 1. Escape probabilities for molecule and dust photons versus the line average optical depth.

$$S = \frac{2h\nu^3}{c^2} \frac{1}{\frac{g_u x_l}{g_l x_u} - 1} \quad (7)$$

u and l denote the upper and lower level of the transition, and τ is the wavelength dependent molecular optical depth:

$$\tau(\nu) = Nx_u \phi(\nu) \frac{A_{ul}}{4\pi} \frac{h\nu}{S} \quad (8)$$

N is the molecular column density, and $\phi(\nu)$ the normalized doppler profile resulting from the velocity distribution of the molecules. In the most general case of our approximations, the profile averaged radiation density used in Equ. 4 (statistical equilibrium) reads:

$$\langle I_\nu \rangle \simeq S(1 - \beta_m) + \frac{F_d}{2} \beta_d \quad (9)$$

where the escape probabilities for molecule and dust photons read:

$$\begin{aligned} \beta_m(\langle \tau \rangle) &= \int \exp(-\tau(\nu)/2) \phi(\nu) d\nu \\ \beta_d(\langle \tau \rangle) &= \int \frac{1 - \exp(-\tau(\nu)/2)}{\tau(\nu)/2} \phi(\nu) d\nu \end{aligned} \quad (10)$$

The factor 2 in Equ. 9 and 10 arises from the fact that, on average, the column density surrounding any point within the cloud is half that seen by the observer.

β_m and β_d have been computed numerically for a Maxwellian velocity distribution. They are plotted in Fig. 1 as a function of the average line optical depth:

$$\langle \tau \rangle = \frac{N}{DV} \frac{c}{\nu} x_u \frac{A_{ul}}{4\pi} \frac{h\nu}{S} \quad (11)$$

where DV is the width of the projected velocity distribution and S the source function.

Finally, the integrated intensity of the lines are computed by evaluating the power radiated by the molecules. Normalized to the velocity width it reads:

$$\begin{aligned} \frac{P_{ul}}{W m^{-2} sr^{-1} (km/s)^{-1}} &= \frac{N}{DV} \frac{h\nu}{4\pi} (x_u R_{ul} - x_l R_{lu}) \\ &= \frac{\nu}{c} \langle \tau \rangle (\beta_m S - \frac{F_d}{2} \beta_d) \end{aligned} \quad (12)$$

Table 3. Calculated population fractions of the lower rotational levels of H_2O ($T = 120\text{K}$, $n_{H_2} = 10^4 \text{cm}^{-3}$, $N_{H_2O} = 10^{16} \text{cm}^{-2}(\text{km/s})^{-1}$, ortho/para = 3). Column 4: ratio of the level population fraction to the population obtained with a pure collisional model.

a) *ortho* – H_2O

$Energy$ [cm^{-1}]	state $v \ JK^-K^+$	fraction in state	fraction /fraction(Coll.)
23.8	000 1 0 1	8.75e-01	1.0
42.4	000 1 1 0	9.18e-02	0.9
79.5	000 2 1 2	3.21e-02	2.5
134.9	000 2 2 1	2.59e-04	100.3
136.8	000 3 0 3	3.58e-04	25.9
173.4	000 3 1 2	1.53e-05	66.4
212.2	000 3 2 1	1.20e-05	225.5
224.8	000 4 1 4	1.19e-07	4.8
285.4	000 3 3 0	4.47e-08	656.7

b) *para* – H_2O

$Energy$ [cm^{-1}]	state $v \ JK^-K^+$	fraction in state	fraction /fraction(coll.)
0.0	000 0 0 0	8.68E-01	0.9
37.1	000 1 1 1	1.19e-01	2.0
70.1	000 2 0 2	1.18e-02	15.7
95.2	000 2 1 1	6.35e-04	237.6
136.2	000 2 2 0	5.63e-05	136.9
142.3	000 3 1 3	1.08e-05	37.7
206.3	000 3 2 2	1.35e-07	251.4
222.1	000 4 0 4	2.55e-08	1.2
275.5	000 4 1 3	1.12e-09	2.7
285.2	000 3 3 1	2.63e-08	648.0

We have run the model for H_2O and NH_3 , two polar molecules likely to be abundant in PDRs because they are expected to be formed in grain mantles and released to the gas in such regions (see e.g. Shalabiea and Greenberg 1994). The physical parameters of the regions are typical of a PDR in a region of high mass star formation (first line in Table 2). Concerning the dust spectrum, we have used the model of Désert et al. (1990) in the case of dust irradiation by an O star. The dust flux has been scaled so that the peak $6.2 \mu\text{m}$ brightness is $3 \cdot 10^4 \text{MJy/sr}$. This is the value expected for this type of PDRs, on the basis of the $3.3 \mu\text{m}$ feature flux measured toward M17 south-west and the Orion bar (Giard et al. 1994b). The ISO-SWS spectrum of Verstraete et al (1996) on the interface region in M17 is about a factor of 15 below the above surface brightness, because of dilution in the ISO-SWS aperture ($14'' \times 20''$) and averaging over 3 different positions.

The coupled system of Eqs. 4 and 9, statistical equilibrium and radiative transfer, have been solved numerically for each molecule, varying the hydrogen density and the molecule column density. We selected the 16 lower rotation levels in each vibration state of the molecule studied. The collision de-excitation rates for transitions between rotation levels in the ground vibration state are taken from Green et al. (1993) for H_2O , and Danby et al. (1988) for NH_3 . Concerning the collision de-excitation rates between different vibration states, we

Table 4. Calculated population fractions of the lower rotational levels of NH_3 ($T = 120\text{K}$, $n_{H_2} = 10^4 \text{cm}^{-3}$, $N_{NH_3} = 10^{15} \text{cm}^{-2}(\text{km/s})^{-1}$, ortho/para = 2). Same as Table 3.

a) *ortho* – NH_3

$Energy$ [cm^{-1}]	state $v \ JK\pm$	fraction in state	fraction /fraction(coll.)
0.4	0000 0 0-	2.59e-01	0.9
19.5	0000 1 0+	7.95e-02	1.8
60.0	0000 2 0-	1.19e-03	10.6
85.9	0000 3 3-	3.04e-01	1.0
86.7	0000 3 3+	3.07e-01	1.0
118.8	0000 3 0+	1.57e-06	3.8
165.3	0000 4 3-	4.09e-04	11.2
166.1	0000 4 3+	3.89e-04	18.0

b) *para* – NH_3

$Energy$ [cm^{-1}]	state $v \ JK\pm$	fraction in state	fraction /fraction(coll.)
16.2	0000 1 1-	2.65e-01	1.0
17.0	0000 1 1+	2.45e-01	1.0
44.8	0000 2 2+	1.97e-01	1.0
45.6	0000 2 2-	1.80e-01	1.0
55.9	0000 2 1-	9.80e-04	3.2
56.7	0000 2 1+	1.01e-03	3.2
104.4	0000 3 2+	1.60e-04	10.1
105.2	0000 3 2-	1.81e-04	10.4
115.5	0000 3 1-	2.88e-06	3.9
116.3	0000 3 1+	2.61e-06	3.9

have assumed the rate value of the same rotation states within the fundamental vibration state. Collision rates values are not critical since, for the temperature and densities considered, $T = 120\text{K}$, $10^2 \text{cm}^{-3} < n_{H_2} < 10^7 \text{cm}^{-3}$, the transitions between two different vibration states are largely dominated by the radiative rates. The line frequencies and the Einstein coefficients are taken from the GEISA data bank (see Husson et al. 1992). As each of the two molecules considered, H_2O and NH_3 , have an ortho and para configuration which are not coupled, we have actually run the model for four different molecular species. We have considered two vibration states for H_2O : 000 (0cm^{-1}) and 010 (1620cm^{-1}), three in the case of NH_3 : 0000 (0cm^{-1}), 0100 (950cm^{-1}) and 0001 (1637cm^{-1}).

4. Results

The population fraction of the rotation levels in the ground vibration state are presented in Tables 3 a, b and 4 a, b for column densities of $10^{16} \text{cm}^{-2}(\text{km/s})^{-1}$ (H_2O) and $10^{15} \text{cm}^{-2}(\text{km/s})^{-1}$ (NH_3), and statistical ortho to para ratio of 3:1 for H_2O and 2:1 for NH_3 . Given the typical hydrogen column density of a PDR, $2N_{H_2} \simeq 10^{21} \text{cm}^{-2}(\text{km/s})^{-1}$ ($2 < A_V < 5$ over 5 km/s, see Tielens and Hollenbach 1985), such molecular column densities correspond to abundances of 10^{-5} and 10^{-6} for H_2O and NH_3 respectively.

Table 5. Calculated intensities of the brighter H_2O lines. ($T = 120\text{K}$, $n_{H_2} = 10^4 \text{ cm}^{-3}$, $N_{H_2O} = 10^{16} \text{ cm}^{-2}(\text{km/s})^{-1}$, ortho/para = 3). Column 1: wavelength in micrometer; column 2: Einstein coefficient; column 3: line intensity; column 4: ratio of the level population fraction to the population obtained with a pure collisional model.

λ [μm]	A_{ij} [s^{-1}]	F [$\text{Wm}^{-2}\text{sr}^{-1}(\text{km/s})^{-1}$]	F /F(coll.)	Upper $v \ JK^-K^+$	Lower $v \ JK^-K^+$
a) ortho – H_2O					
538.289	3.6e-03	2.51e-10	0.9	000 1 1 0	000 1 0 1
273.193	1.7e-02	1.00e-09	59.2	000 3 1 2	000 3 0 3
259.984	3.9e-03	2.63e-10	64.7	000 3 1 2	000 2 2 1
257.791	2.4e-02	1.30e-09	225.2	000 3 2 1	000 3 1 2
180.488	3.2e-02	2.21e-09	25.9	000 2 2 1	000 2 1 2
179.526	9.7e-02	3.37e-09	2.3	000 2 1 2	000 1 0 1
174.626	7.4e-02	1.89e-09	7.3	000 3 0 3	000 2 1 2
75.380	4.8e-01	-4.17e-09	-119.2	000 3 2 1	000 2 1 2
6.642	7.4e+00	4.51e-08		010 1 1 0	000 2 2 1
6.185	1.0e+01	-4.84e-08		010 1 1 0	000 1 0 1
b) para – H_2O					
398.643	7.3e-03	1.07e-09	62.1	000 2 1 1	000 2 0 2
303.459	1.0e-02	1.87e-09	7.4	000 2 0 2	000 1 1 1
269.273	5.7e-02	1.50e-09	2.1	000 1 1 1	000 0 0 0
243.972	1.9e-02	1.68e-09	129.5	000 2 2 0	000 2 1 1
138.527	1.8e-01	1.98e-10	1.6	000 3 1 3	000 2 0 2
100.983	4.5e-01	-2.32e-09	-226.0	000 2 2 0	000 1 1 1
67.089	1.8e+00	1.81e-10	423.5	000 3 3 1	000 2 2 0
46.484	3.0e-02	-2.47e-10	-2.4e+04	000 3 3 1	000 2 0 2
6.672	6.3e+00	2.34e-08		010 1 1 1	000 2 2 0
6.390	3.0e+00	1.16e-08		010 1 1 1	000 2 0 2
6.116	2.1e+01	-3.80e-08		010 1 1 1	000 0 0 0

Table 6. Calculated intensities of the brighter NH_3 lines. ($T = 120K$, $n_{H_2} = 10^4 cm^{-3}$, $N_{NH_3} = 10^{15} cm^{-2}(km/s)^{-1}$, ortho/para = 2). Same as Table 5.

λ [μm]	A_{ij} [s^{-1}]	F [$Wm^{-2}sr^{-1}(km/s)^{-1}$]	F /F(coll.)	Upper $v JK\pm$	Lower $v JK\pm$
a) ortho – NH_3					
523.670	9.5e-03	3.15e-10	2.2	0000 1 0+	0000 0 0-
246.773	6.1e-02	6.09e-10	4.6	0000 2 0-	0000 1 0+
169.996	1.7e-01	1.17e-10	2.8	0000 3 0+	0000 2 0-
127.108	8.4e-02	2.92e-10	2.6	0000 4 3-	0000 3 3+
124.648	8.8e-02	2.71e-10	3.7	0000 4 3+	0000 3 3-
11.209	1.0e+01	9.09e-09		0100 1 0+	0000 2 0-
10.507	3.1e+01	-9.64e-09		0100 1 0+	0000 0 0-
b) para – NH_3					
256.575	2.0e-02	1.20e-10	2.2	0000 2 1-	0000 1 1+
246.694	2.3e-02	1.25e-10	2.2	0000 2 1+	0000 1 1-
169.990	7.5e-02	5.92e-11	3.5	0000 3 1-	0000 2 1+
169.967	4.7e-02	8.91e-11	2.7	0000 3 2+	0000 2 2-
165.728	8.1e-02	5.92e-11	3.5	0000 3 1+	0000 2 1-
165.596	5.0e-02	9.08e-11	2.6	0000 3 2-	0000 2 2+
11.460	4.5e+00	6.04e-10		0100 2 1-	0000 3 1+
11.011	5.1e+00	6.46e-10		0100 2 1+	0000 3 1-
10.289	8.2e+00	-1.03e-09		0100 2 1-	0000 1 1+
9.925	9.2e+00	-1.13e-09		0100 2 1+	0000 1 1-

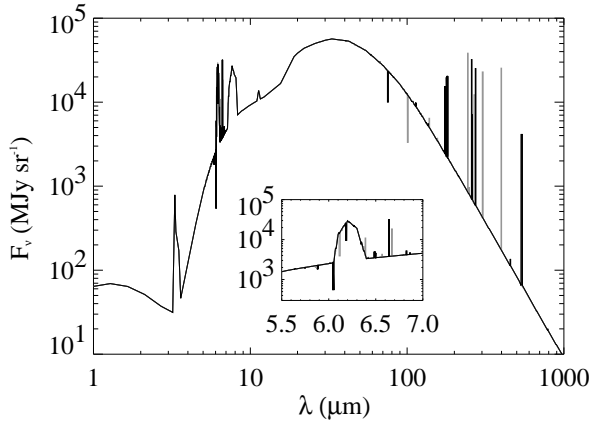


Fig. 2. Synthetic dust plus H_2O spectrum emerging from the PDR (dashed lines for para species). $T = 120\text{K}$, $n_{H_2} = 10^4\text{ cm}^{-3}$, $N_{H_2O} = 10^{16}\text{ cm}^{-2}(\text{km/s})^{-1}$, ortho/para = 3.

Except the peculiar case of the NH_3 metastable levels ($J = K$, see Sect. 4.2), the population fractions are far from thermal equilibrium, because the density used does not allow collisional excitation rates to overwhelm spontaneous radiative emission (critical H_2 density $\simeq 10^8\text{ cm}^{-3}$ for excitation of a 100 cm^{-1} level of NH_3 or H_2O in a 100K gas). For this reason we compare the results of our model to a pure collisional model where the dust flux has been set to zero (Column 4 in Tables 3a, b and 4a, b).

The predicted intensities of the brightest H_2O and NH_3 lines are listed in Tables 5a,b and 6a,b. Fig. 2 and 4 display the calculated synthetic infrared spectra emerging from the PDR. In these plots, the height of each line above or below the continuum is not proportional to its integrated intensity, because the different optical depths of the lines induce different line widths. The insert shows the details of the expected NIR vibration transitions.

Our results show that the net effect of the NIR pumping is to slightly reduce the fraction of molecules in the lowest rotation level, increasing the population of the excited levels and thus increasing the intensities of the submillimeter and far infrared lines. However, the detailed behaviours for H_2O and NH_3 are not the same, because of the different radiative selection rules.

4.1. H_2O

H_2O is an asymmetric top with a dipole moment of 1.94 Debye. We refer to the rotation levels of H_2O using the general $J_{K^-K^+}$ numbering of the asymmetric top molecules, where J is the total angular momentum and K^- (respectively K^+) is the projection of the angular momentum on the symmetry axis for the limiting prolate (respectively oblate) molecule (see Townes and Shallow 1975). The selection rules are, $\Delta J = 0, +1, -1$ and $\Delta(K^- - K^+)$ even. The later rule forbids para/ortho radiative transitions since $K^- - K^+$ is odd for ortho and even for para - H_2O .

As can be seen from Fig. 3a, the excitation scheme for ortho - H_2O is quite complex because of the combination of the radiative pumping by NIR photons in the vibrational transitions and FIR photons in the rotational transitions. The

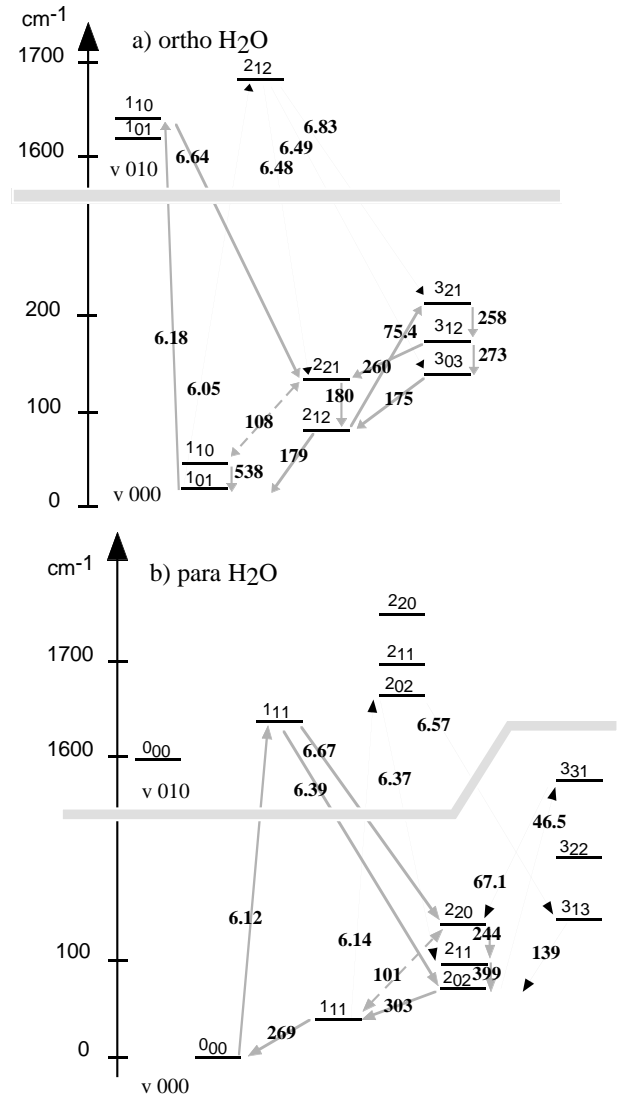


Fig. 3. Levels and main radiative transitions for a) ortho and b) para H_2O . The wavelength of each transition in micron is indicated in bold characters. (Thick arrows for the stronger transitions).

molecule is mostly excited by NIR pumping in the $v010\ 1_{10}$ level and subsequent deexcitation in the 2_{21} rotation level of the vibration ground state (absorption at $6.18\ \mu\text{m}$ and emission at $6.64\ \mu\text{m}$). The population fraction of the $v000\ 2_{21}$ level is considerably increased with respect to the comparison model ($\simeq 100$). Two different de-excitation channels are possible from this level. The first one through the $108\ \mu\text{m}(2_{21} - 1_{10})$ line, and the second one through the $180.5\ \mu\text{m}(2_{21} - 2_{12})$ line. The first channel is not efficient because for the parameters we have selected, $n_{H_2} = 10^4\text{ cm}^{-3}$ and $\frac{N_{H_2O}}{DV} = 10^{16}\text{ cm}^{-2}(\text{km/s})^{-1}$, emission in the $108\ \mu\text{m}$ line is balanced by radiative pumping by FIR dust photons in the same line. Thus, the de-excitation occurs mainly through the $180.5\ \mu\text{m}$ line. The intensity of this line is increased by a factor of order 25 with respect to the collision model. Once in level 2_{12} , the molecule may either be excited in the 3_{21} level by absorption of a $75.4\ \mu\text{m}$ dust pho-

ton, or de-excited in the ground level (1_{01}) by emission at $179.5 \mu\text{m}$. The population fractions of the $J=3$ ladder are increased by one to two decades with respect to the collisional model. Consequently, the intensities of the FIR and submillimeter de-excitation lines are enhanced by similar factors. NIR pumping at $6.18 \mu\text{m}$ has thus a major effect on the $(2_{21} - 2_{12})$ line at $180.5 \mu\text{m}$, whereas FIR pumping at $75.4 \mu\text{m}$ mostly enhances the following transitions: $(3_{21} - 3_{12})$ at $258 \mu\text{m}$, $(3_{12} - 2_{21})$ at $260 \mu\text{m}$, $(3_{12} - 3_{03})$ at $273 \mu\text{m}$, and $(3_{03} - 2_{12})$ at $175 \mu\text{m}$.

The intensity of the $108 \mu\text{m}$ line is driven both by NIR and FIR pumping, and this line can appear in emission or absorption against the dust continuum, depending on the radiation field, the gas density and the molecular column density (see Fig6b).

The case of *para* - H_2O is quite similar to *ortho* - H_2O . The main NIR absorption line, $(0_{00} - 1_{11})$, is located at $6.12 \mu\text{m}$, with re-emissions predicted at 6.39 and $6.67 \mu\text{m}$ (see Fig. 3b), populating mainly the $J=2$ rotation ladder. Excitation of the $J=3$ ladder is much less efficient than in the case the *ortho* species because the allowed transition has a low Einstein coefficient ($3 \cdot 10^{-2}$ against 0.48 for the $75.4 \mu\text{m}$ line of *ortho* - H_2O). NIR and FIR pumping are thus responsible for bright de-excitation lines in the $J=2$ ladder: $(2_{20} - 2_{11})$ at $244 \mu\text{m}$, $(2_{11} - 2_{02})$ at $399 \mu\text{m}$ and $(2_{02} - 1_{11})$ at $303 \mu\text{m}$. As for the *ortho* - H_2O $108 \mu\text{m}$ line, the $(2_{20} - 1_{11})$ line at $101 \mu\text{m}$ will appear either in absorption or emission on the continuum, depending on the physical parameters of the region.

In the regime where the NIR pumping line is not saturated ($N_{H_2O} < 10^{16} \text{cm}^{-2}(\text{km/s})^{-1}$) the absorptions at 6.18 and $6.12 \mu\text{m}$ give a direct estimate of the *ortho* and *para* column densities. Furthermore, FIR lines will increase with the pumping rate, i.e. the radiation field. This later parameter can be fairly well known by direct observation of the dust and PAH NIR spectrum. Once this is done, the intensities of the FIR lines can be used to trace the molecule column densities. This is shown in Fig. 6a where the calculated iso-intensities of the $180.5 \mu\text{m}$ ($2_{21} - 2_{12}$) line are drawn versus the H_2O column density and the H_2 density. The dotted contours in the same plot correspond to the comparison model (collisions only). In the comparison model the line intensity increases fairly regularly with the gas density and the molecule column density. If radiative pumping is introduced as in our model, it dominates the excitation at moderate densities, $n_{H_2} < 10^5 \text{cm}^{-3}$, so long as the $6.18 \mu\text{m}$ pumping line is optically thin: $N_{H_2O} < 10^{16} \text{cm}^{-2}(\text{km/s})^{-1}$. In this domain of the parameter space, which is appropriate for the conditions that prevail within PDRs, the line intensity is almost independent of the gas density and can be used to trace the column density. However, for the $180.5 \mu\text{m}$ line, the intensity is not a linear function of the column density. This is because the upper and lower levels of the transition have several other radiative exciting or deexciting channels which become optically thick in different column density ranges.

Fig. 6b shows the intensity contours of the $(2_{21} - 1_{10})$ $108 \mu\text{m}$ *ortho* - H_2O line. For the sake of clarity we didn't overplot the contours obtained with the comparison model. They are quite similar to those of the $180.5 \mu\text{m}$ line in Fig. 6a. As mentioned above, this line appears either in absorption or emission, depending on the gas density, the molecule column density and the radiation field. Including NIR pumping favors emission in this line since the upper level is directly fed by the de-excitation of the excited vibration state. This

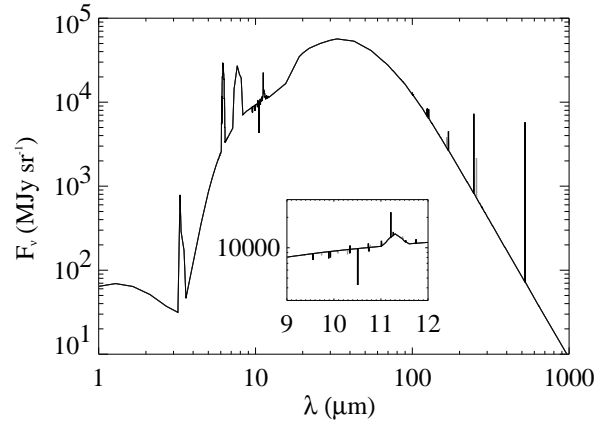


Fig. 4. Synthetic dust plus NH_3 spectrum emerging from the PDR. Same as Fig. 2. $T = 120\text{K}$, $n_{H_2} = 10^4 \text{cm}^{-3}$, $N_{NH_3} = 10^{15} \text{cm}^{-2}(\text{km/s})^{-1}$, *ortho/para* = 2.

is why the domain where the line will appear in absorption against the dust continuum is restricted to a small region: $10^{14} < N_{H_2O} < 10^{16} \text{cm}^{-2}(\text{km/s})^{-1}$, $10^4 < N_{H_2} < 10^6 \text{cm}^{-3}$.

It is worth pointing out that, in addition to increasing considerably the H_2O submillimeter and FIR line intensities, radiative pumping will strongly modify the lines intensity ratios with respect to pure collisional models. For instance, the $180.5 \mu\text{m}$ to $179.5 \mu\text{m}$ *ortho* - H_2O line intensity ratio is increased by a factor of order 10, and the $398 \mu\text{m}$ *para* - H_2O to $538 \mu\text{m}$ *ortho* - H_2O submillimeter lines ratio is enhanced by a factor of 60. Such effects have very important observational consequences, particularly when the lines are used to derive column densities and *ortho* to *para* abundance ratios.

Finally, the NIR lines predicted to appear in absorption and emission against the PAH continuum can directly be used to probe the H_2O column density. The line to continuum contrast of the emission transitions is high (see insert in Fig. 2), because the intensity of these lines comes from energy absorbed at the maximum of the $6.2 \mu\text{m}$ PAH band. With *ortho* - H_2O , we actually have a case of quasi-resonant excitation. The primary emission transition at $6.64 \mu\text{m}$ is thus a good target for observations. For instance, if we assume a line width of 10km/s , the measured line to continuum contrast is still of order 50% in the $6.64 \mu\text{m}$ transition, after dilution by the ISO-SWS grating spectral resolution ($R \simeq 1500$). This is to be compared to the contrast in the absorption line at $6.18 \mu\text{m}$, $\simeq 5\%$ for the same resolution.

4.2. NH_3

NH_3 is a symmetric top prolate rotator with a dipole of 1.47 Debye. The possible tunnelling of the nitrogen nucleus through the hydrogen plan is responsible for the inversion splitting of the rotation levels with $K \neq 0$ (levels + and -). We refer to the levels using the usual $J, K \pm$ numbering (see Townes and Shallow 1975). An additional quantum number due to a rotation-vibration interaction, $l = \pm 1$, appears in the case of the degenerate vibration states (e.g. 0001). The selection rules are those of a symmetric top: $\Delta J = 0, +1, -1$; $+\leftrightarrow -$; and $\Delta K = 0$ for transitions which do not involve a degenerate vibration state. The later rule implies that the different K ladders are not ra-

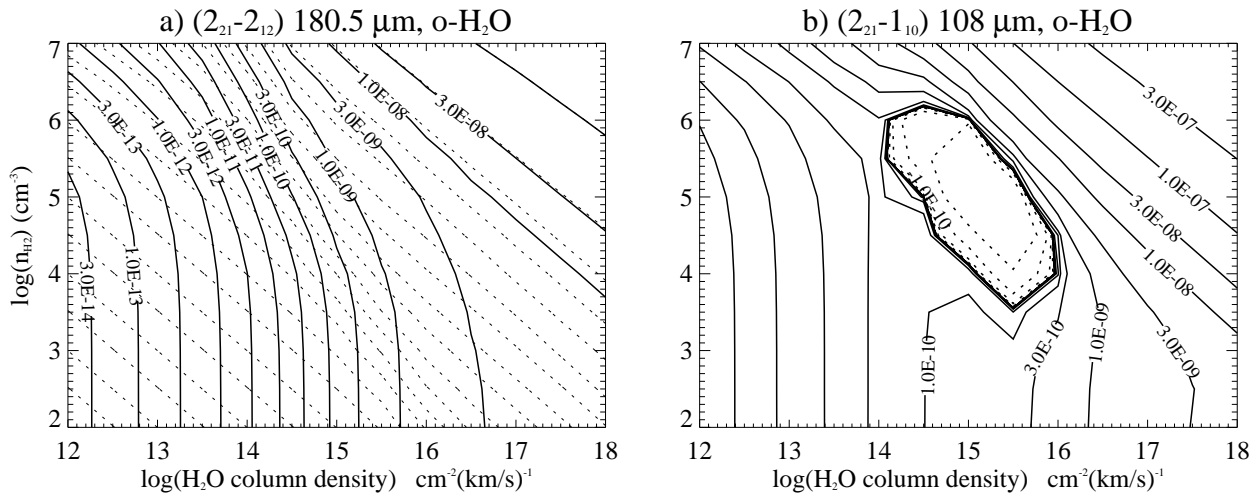


Fig. 6. iso-intensities of a) *ortho* - H_2O ($2_{21} - 2_{12}$) $180.5 \mu m$ and b) *ortho* - H_2O ($2_{21} - 1_{10}$) $108 \mu m$ lines as a function of the molecule column density and the hydrogen density. Dotted lines in a) are the contours obtained with a pure collisional model. Dotted lines in b) for an absorption line. Units are $W m^{-2} sr^{-1} (km/s)^{-1}$.

In addition to H_2O and NH_3 one can list CS , HCN , CO_2 , CH_4 , H_3O^+ , HC_3N , and CH_3OH . The combination of the absorption and emission lines from all species existing in the gas phase is likely to be responsible for the very complex detailed structure of the 5 to 20 μm spectra measured at moderate spectral resolution in the direction of the M17-SW PDR with the ISO-SWS instrument (Verstraete et al. 1996). Decrypting such spectra in terms of molecular abundances will require the production of synthetic model spectra including a significant number of molecules of astrophysical interest. This will be done in a forthcoming paper.

Acknowledgements. We are grateful to B. Bonnet and N. Husson for making available to us the full GEISA file.

References

- Boulanger, F., Reach, W.T., Abergel, A., Bernard, J.P., Cesarsky, C.J., Cesarsky, D., Désert, F.X., Falgarone, E., Lequeux, J., Metcalfe, L., Péroul, M., Puget, J.L., Rouan, D., Sauvage, M., Tran, D., and Vigroux, L., A&A 315, L325
 Carroll, T.J., and Goldsmith, P.F., 1981, ApJ 245, 891
 Collison, A.J., and Watson, W.D., 1995, ApJ 452, L103
 Danby, G., Flower, D.R., Valiron, P., Schilke, P., and Walmsley, C.M., 1988, MNRAS 235, 239
 Désert, F.X., Boulanger, F., and Puget, J.L., 1990, A&A 237, 215
 Encrenaz T., Crovisier, J., d'Hendecourt, L., Lamy, P., and Tully, J.A., 1992, in "Infrared Astronomy with ISO", Eds Encrenaz T. and Kessler, M., Nova Science Publishers, Inc., p 141
 Genzel, R., Harris, A.I., Jaffe, D.T. and Stutzki, J., 1988, ApJ 332, 1049
 Giard, M., Bernard, J.P., and Deneffeld, M., 1992, A&A 264, 610
 Giard, M., Lamarre, J.M., Pajot, F., and Serra, G., 1994a, A&A 286, 203
 Giard, M., Bernard, J.P., Lacombe, F., Normand, P., and Rouan, D., 1994b, A&A 291, 239

- Goldreich, P., and Kwan, J., 1974, ApJ 189, 441
 Goldsmith, P.F., and Langer, W.D., 1978, ApJ 222, 881
 Green, S., Maluendes, S., and McLean, A.D., 1993, ApJ Sup., 85, 181
 Husson, N., Bonnet, B., Scott, N., and Chedin, A., 1992, J. Quant. Spec. Rad. Tr. 48-5/6, 509
 Mattila, K., Lemke, D., Haikala, L.K., Laureijs, R.J., Léger, A., Lehtinen, K., Leinert, Ch., and Mezger, P.G., 1996, A&A 315, L353
 Phillips, T.G., Van Dishoeck, E.F., and Keene, J., 1992, ApJ 399, 533
 Puget, J.L., Léger, A. and Boulanger, F., 1985, A&A 142, L19
 Rieke, G.H. and Lebofsky, M.J., 1985, ApJ 288, 618
 Ristorcelli, I., Giard M., Mény C., Serra G., Lamarre, J.M., Le Naour, C., Léotin, J., and Pajot, F., A&A 286, L23
 Shalabiea, O.M., and Greenberg, J.M., 1994, A&A 290, 266
 Stutzki, J., Stacey, G.J., Genzel, R., Harris, A.I., Jaffe, D.T., and Lugten, J.B., 1988, ApJ 332, 379
 Takahashi, T., Hollenbach, D.J., and Silk, J., 1983, ApJ 275, 145
 Takahashi, T., Hollenbach, D.J., and Silk, J., 1985, ApJ 292, 192
 Tielens, A.G.G.M., and Hollenbach, D., 1985, ApJ 291, 722
 Tielens, A.G.G.M., Meixner, M.M., van der Werf, P.P., Bregman, J., Tauber, J.A., Stutzki, J., and Rank, D., 1993, Science 262, 86
 Townes, C.H., and Shawlow, A.L., 1955, in "Microwave spectroscopy", Eds. Dover
 Verstraete, L., Puget, J.L., Falgarone, E., Drapatz, S., Wright, C., and Timmermann, R., 1996, A&A 315, L337